

Safety-Critical Control for Smoothed Implicit Contact Dynamics

Haegun Lee, Yitaek Kim and Christoffer Sloth

Abstract—Smoothed implicit contact dynamics enables gradient-based planning and control for contact-rich tasks without predefined mode sequences. However, safety-critical control remains challenging because implicit contact dynamics makes safety-filter design nontrivial. The smoothing parameter κ relaxes contact complementarity constraints, which makes the dynamics smooth but affects the contact force. This paper provides a method for bounding the actual contact force despite the use of relaxed complementarity constraints. We show that constraint violations can be non-monotonic in κ . Smaller κ reduces force-approximation error, but it does not necessarily improve safety performance. To address this issue, we introduce boundary-focused rollouts to screen κ by comparing the safety margin with the approximation error. We then develop a discrete-time control barrier function (CBF) framework based on a first-order Taylor approximation of the implicitly defined contact force. To account for possible force under-prediction, we augment the resulting safety constraint with a fixed robust margin. Simulations on four contact-rich systems show that the proposed method eliminates force violations observed under a standard CBF.

I. INTRODUCTION

Robotic systems that undergo intermittent contact interaction with the environment are difficult to plan because their contact modes change over time [1], [2]. Explicit hybrid contact models often rely on predefined mode sequences or on resolving contact modes online [3], [4], both of which can be nontrivial for contact-rich tasks. However, implicit contact dynamics provides an attractive alternative by representing contact within a unified dynamics framework without requiring predefined mode sequences. Implicit contact dynamics has facilitated trajectory planning through contact in several recent works [5], [6], [7], [8].

Contact dynamics are inherently nonsmooth and non-differentiable, which makes them difficult to handle with gradient-based methods. A common approach is to smooth the contact dynamics to make it suitable for gradient-based optimization. Existing smoothing methods aim to make the dynamics differentiable [9], [10]. In particular, smoothed contact dynamics have been successfully applied to gradient-based planning through contact [11], [12], [13]. However, these advances have primarily focused on differentiable simulation and planning, rather than safety-critical control.

Safety guarantees are often required in contact-rich control, particularly when tasks involve fragile objects, uncertain contact conditions, and human-robot interaction. Recent studies have incorporated force-related safety using explicit contact models through interaction-force constraints

All authors are with The Maersk Mc-Kinney Møller Institute, University of Southern Denmark, Denmark {haeg, yik, chsl}@mmmi.sdu.dk

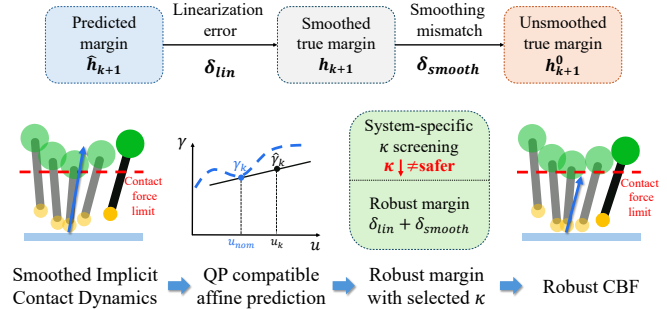


Fig. 1: Illustration of the proposed robust CBF framework for smoothed implicit contact dynamics. A local Taylor approximation gives a QP-compatible safety prediction, while system-specific κ screening and robust margin tightening compensate for linearization error and smoothing mismatch.

and CBF-based safety filtering [14], [15], [16]. Robust CBF formulations have also been developed to account for disturbances and uncertainty in the system dynamics [17], [18]. However, these approaches rely on explicit models whose dynamics are often control-affine and therefore readily compatible with standard CBF formulations.

Recent advances in differentiable physics engines have enabled efficient gradient-based simulation and optimization for contact-rich robotic systems [19], [20], [21]. Among these approaches, formulations based on Nonlinear Complementarity Problems (NCPs) with second-order cone constraints provide accurate and differentiable simulation of implicit contact dynamics [10]. Although these models have shown strong performance in trajectory optimization and planning through contact [22], formal safety guarantees for the strict enforcement of contact-force constraints remain limited. This is because implicit contact models are generally non-affine in the control input. As a result, standard CBF formulations for control-affine systems cannot be applied directly [23], [24], [25]. Although several studies have considered safety for non-affine systems [26], [27], [28], they do not directly address implicit contact dynamics governed by complementarity constraints. Therefore, ensuring contact-force safety under implicit contact dynamics remains an open challenge.

In this paper, we make three main contributions:

- 1) We formulate contact-force safety filtering for smoothed implicit contact dynamics using discrete-time control barrier functions, where the safety set is defined by contact-force constraints.
- 2) We characterize how the smoothing parameter κ affects the CBF safety condition by relating the predicted safety margin to the one-step error induced by a local approximation of the implicit contact force. This

analysis shows that a smaller smoothing parameter can improve local contact-model accuracy while still degrading the reliability of the safety filter.

- 3) We propose a robust safety filter that bounds the unsmoothed contact force despite using relaxed complementarity constraints by tightening the predicted CBF condition with conservative margins for both linearization error and smoothing mismatch.

Simulation results across multiple contact-rich systems show that the proposed method reduces contact-force constraint violations relative to a standard CBF formulation.

II. PRELIMINARIES AND PROBLEM FORMULATION

In this section, we briefly review the implicit contact dynamics model and discrete-time control barrier functions used in the proposed safety filter.

A. Contact Dynamics Model

Accurate modeling of contact forces is important when robots interact with environments. This paper adopts the complementarity-based contact dynamics model of [10], in which contact and friction are modeled using a Nonlinear Complementarity Problem (NCP).

Let $\phi : \mathcal{Z} \rightarrow \mathbb{R}$ be the signed-distance function, where \mathcal{Z} denotes the configuration space. The normal contact force at time step k is denoted by γ_k . In the discrete-time setting, a central-path parameter $\kappa > 0$ is introduced to relax the hard complementarity condition. The resulting unilateral contact conditions at configuration $z \in \mathcal{Z}$ are

$$\phi(z) \geq 0, \quad (1a)$$

$$\gamma \geq 0, \quad (1b)$$

$$\gamma\phi(z) = \kappa. \quad (1c)$$

These conditions enforce non-penetration and unilateral contact while replacing the hard complementarity relation ($\kappa = 0$) with a smooth central-path condition ($\kappa > 0$). Fig. 2 illustrates the resulting effect on local contact sensitivity in a one-dimensional box contact example. In the nonsmooth model, the contact-force sensitivity with respect to the vertical input force changes abruptly near lift-off, whereas the smoothed model produces a differentiable transition whose sensitivity depends on κ .

Frictional contact is modeled using the relative tangential velocity v_{k+1} between the objects in contact and tangential contact impulse β_{k+1} at the contact point. In the discrete-time setting, Coulomb friction is derived from the maximum dissipation principle, which yields

$$\begin{aligned} \min_{\beta_{k+1}} \quad & v_{k+1}^\top \beta_{k+1} \\ \text{s.t.} \quad & \|\beta_{k+1}\|_2 \leq \mu \gamma_{k+1}, \end{aligned} \quad (2)$$

where μ is the coefficient of friction.

Together with the unilateral contact condition (1) and the friction-cone constraint (2), this defines the contact update at time step k as a nonlinear complementarity problem. Let

$$\theta_k := (z_{k-1}, z_k, u_k), \quad w_k := (z_{k+1}, \gamma_{k+1}, \beta_{k+1}), \quad (3)$$

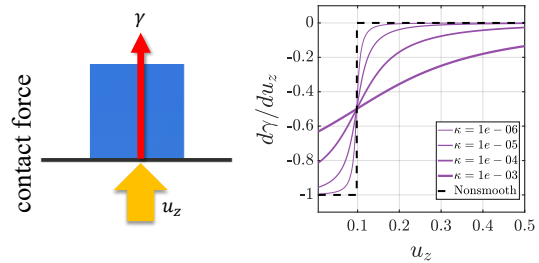


Fig. 2: Gradients are computed for different values of the central-path parameter κ . The dynamics involve a box of mass 0.01 kg resting on a flat surface in the XZ plane. The applied force was gradually increased from 0 N to 0.5 N.

where θ_k denotes the problem data at time step k , and w_k denotes the corresponding solution.

The relaxed implicit contact dynamics can be written compactly as

$$r(w_k; \theta_k, \kappa) = 0. \quad (4)$$

Let w_k^* denote a solution to (4). Since the relaxed problem is smooth, local sensitivities with respect to the problem data θ_k and parameter κ can be computed by implicit differentiation [29]:

$$\frac{\partial w_k^*}{\partial \xi} = - \left(\frac{\partial r}{\partial w_k} \right)^{-1} \frac{\partial r}{\partial \xi}, \quad \xi \in \{\theta_k, \kappa\}. \quad (5)$$

The contact force component of this sensitivity later provides the local input derivative needed to formulate QP-compatible CBF constraints.

B. Control Barrier Functions

Consider the following control system with explicit dynamics

$$x_{k+1} = f(x_k, u_k) \quad (6)$$

where $x_k \in \mathcal{X} \subset \mathbb{R}^n$ consists of z_k and v_k , and $f : \mathcal{X} \times \mathcal{U} \rightarrow \mathbb{R}^n$ is locally Lipschitz. The safe set is defined as the 0-superlevel set of a continuously differentiable function $h : \mathbb{R}^n \rightarrow \mathbb{R}$:

$$\mathcal{S} = \{x \in \mathcal{X} \mid h(x) \geq 0\}. \quad (7)$$

For system (6), the continuously differentiable function h is a discrete-time control barrier function [25] if $\frac{\partial h}{\partial x} \neq 0$ for all $x \in \partial \mathcal{S}$, and there exists $\alpha \in [0, 1]$ such that for all x ,

$$h_{k+1} \geq (1 - \alpha)h_k, \quad (8)$$

where $h_k := h(x_k)$ and $h_{k+1} := h(x_{k+1})$. If condition (8) is satisfied, the lower bound of $h(x_k)$ decays exponentially with rate $(1 - \alpha)$. This implies that the system is safe with respect to \mathcal{S} for any $x_0 \in \mathcal{S}$ [25].

C. Problem Formulation

This paper considers contact-force safety under smoothed implicit contact dynamics. The goal is to enforce the constraint $\gamma_k \leq \gamma_{\max}$ using a safety filter, while accounting for the fact that the central-path parameter κ changes the relaxed contact response and the resulting safety margin. The problem is to characterize this κ -dependent behavior

and choose a robust margin that makes the local safety-filter prediction reliable near the safety boundary. We also consider how the resulting contact safety guarantee can be extended to the unsmoothed contact dynamics by accounting for the smoothing mismatch.

III. SAFETY-CRITICAL CONTROL WITH IMPLICIT CONTACT DYNAMICS

CBF frameworks typically rely on explicit control-affine system dynamics, allowing safety constraints to be written as quadratic programs (QPs). In our setting, the contact force is defined implicitly through the NCP, so the standard CBF-QP cannot be applied directly. We therefore use a local approximation of the contact force to derive a QP-compatible constraint.

A. Approximation of Implicit Contact Dynamics

Throughout this section, we consider only force constraints of the form $\gamma_k \leq \gamma_{\max}$ for all k ; hence, we define the barrier function as

$$h_k := \gamma_{\max} - \gamma_k, \quad (9)$$

where γ_{\max} denotes the maximum allowable contact force. Condition (8) cannot be enforced directly through a QP because the implicit contact dynamics (4) is not given in the form (6). At this stage, two approaches are possible: 1) Combine the CBF-based safety filter directly with the implicit contact dynamics, which leads to a nonlinear optimization problem that preserves the implicit model structure; 2) Locally linearize the implicitly defined contact force around the nominal input, which yields an affine approximation suitable for a standard CBF-QP.

In this work, we adopt the local approximation approach as it is suited for real-time implementation. At time step k , let u_k^{nom} denote the nominal input from some nominal controller. The local approximation is obtained as a first-order Taylor expansion around u_k^{nom} :

$$\hat{\gamma}_{k+1}(u_k; \kappa) = \gamma_{k+1}^{\text{nom}} + J_{\gamma, k+1}(u_k - u_k^{\text{nom}}) \quad (10)$$

where

$$\gamma_{k+1}^{\text{nom}} := \gamma_{k+1}(u_k^{\text{nom}}; \kappa) \quad (11)$$

and

$$J_{\gamma, k+1} := \left. \frac{\partial \gamma_{k+1}(u_k; \kappa)}{\partial u_k} \right|_{\theta_k = \theta_k^{\text{nom}}, u_k = u_k^{\text{nom}}} \quad (12)$$

The safety-critical input is computed by solving the following CBF-QP:

$$u_k^* = \arg \min_{u_k \in \mathcal{U}} \frac{1}{2} \|u_k - u_k^{\text{nom}}\|^2 \quad (13)$$

$$\text{s.t. } J_{\gamma, k+1} u_k \leq h_{k+1}^{\text{nom}} + J_{\gamma, k+1} u_k^{\text{nom}} - (1 - \alpha) h_k. \quad (14)$$

Here, $J_{\gamma, k+1}$ denotes the local input sensitivity of the next-step contact force, and h_{k+1}^{nom} denotes the next-step safety margin at the nominal input. The derivation of (14) is provided below.

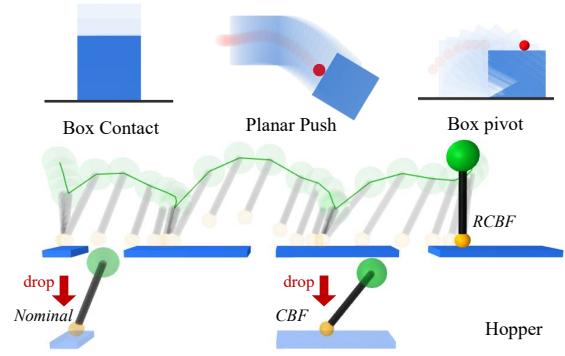


Fig. 3: Overview of the contact-force safety problem under smoothed implicit contact dynamics. The bottom row shows a forward hopping task with a possible terrain drop.

The corresponding first-order prediction is defined as (10). Since safety is considered through the predicted contact force, the approximation error between $\hat{\gamma}_{k+1}$ and γ_{k+1} must be accounted for in the CBF constraint. Thus, we write

$$\gamma_{k+1}(u_k; \kappa) = \hat{\gamma}_{k+1}(u_k; \kappa) + \epsilon_{\gamma, k}(u_k; \kappa), \quad (15)$$

where $\epsilon_{\gamma, k}(u_k; \kappa)$ denotes the higher-order approximation error. For inputs near u_k^{nom} , the higher-order remainder is assumed to satisfy

$$|\epsilon_{\gamma, k}(u_k; \kappa)| \leq \bar{\epsilon}_\gamma(\kappa), \quad (16)$$

where the bound may depend on κ .

The nominal and predicted next-step safety margins are defined as

$$\begin{aligned} h_{k+1}^{\text{nom}} &:= \gamma_{\max} - \gamma_{k+1}^{\text{nom}}, \\ \hat{h}_{k+1}(u_k; \kappa) &:= \gamma_{\max} - \hat{\gamma}_{k+1}(u_k; \kappa). \end{aligned} \quad (17)$$

Using (10), the predicted margin becomes

$$\hat{h}_{k+1}(u_k; \kappa) = h_{k+1}^{\text{nom}} - J_{\gamma, k+1}(u_k - u_k^{\text{nom}}). \quad (18)$$

Neglecting higher-order Taylor terms $\epsilon_{\gamma, k}$, we impose the discrete-time CBF condition on the predicted margin as

$$\hat{h}_{k+1}(u_k; \kappa) \geq (1 - \alpha) h_k. \quad (19)$$

Substituting (18) into (19) directly yields

$$h_{k+1}^{\text{nom}} - J_{\gamma, k+1}(u_k - u_k^{\text{nom}}) \geq (1 - \alpha) h_k, \quad (20)$$

which can be rearranged into the affine CBF constraint in (14). The approximation error induced by the local affine force prediction is accounted for in Sec. III-D through robust tightening.

B. κ -Dependent Safety Margin Analysis

The central-path parameter κ relaxes the complementarity constraints and changes the resulting contact force. Since the barrier function is defined in terms of the contact force, the safety margin also depends on κ through $\gamma_{k+1}(u_k; \kappa)$.

The corresponding safety-margin approximation error is

$$\Delta h_k := h_{k+1} - \hat{h}_{k+1} = -\epsilon_{\gamma, k}(u_k; \kappa). \quad (21)$$

To illustrate the key ideas behind the proposed CBF-based framework for implicit contact dynamics, we first consider

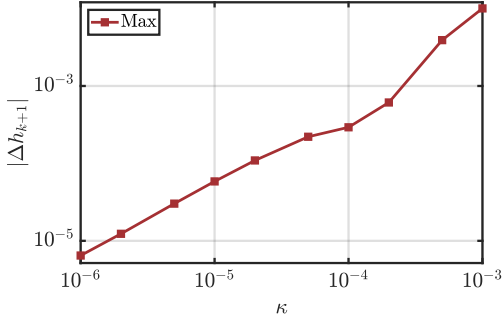


Fig. 4: Absolute safety-margin approximation error $|\Delta h_k| = |h_{k+1} - \hat{h}_{k+1}|$ versus the smoothing parameter κ in the 1D box contact rollout. For each κ , the plot reports the maximum error over rollout steps for which the solved contact force γ_{k+1} is positive.

the simple one-dimensional box contact example shown in Fig. 3. We then extend the evaluation to a broader class of contact-rich systems.

Fig. 4 shows that the one-step approximation error decreases as κ becomes smaller, indicating that smaller κ yields a more accurate local prediction of the safety margin. To investigate how this improved local accuracy affects true safety behavior, the simple one-dimensional box contact example in Fig. 3 is evaluated over a range of κ values. The CBF-QP in (13) is used to filter the nominal input whenever the predicted force exceeds the contact force limit. Fig. 5 shows the resulting contact force trajectories. Among the four tested values of κ at $\gamma_{\max} = 0.25$ N, only $\kappa = 10^{-4}$ remains within the force limit, whereas both smaller and larger values of κ lead to force violations.

To further investigate this result, the evaluation is repeated over 20 values of κ ranging from 10^{-6} to 10^{-3} . Fig. 6(a) shows that the non-violation region appears over an interval of κ near 10^{-4} . This behavior can be understood from the interaction between the predicted safety margin and the approximation error introduced by the local affine approximation. While the CBF-QP enforces the linearized constraint using \hat{h}_{k+1} , true safety depends on

$$h_{k+1} = \hat{h}_{k+1} + \Delta h_k. \quad (22)$$

Consequently, a safety violation occurs whenever

$$\hat{h}_{k+1} + \Delta h_k < 0. \quad (23)$$

Although decreasing κ reduces the approximation error, the empirical results show that safety does not necessarily improve monotonically as κ decreases. To interpret this behavior, we examine the local central-path relation along the κ -dependent closed-loop solution.

Consider a range of positive κ values over which the predicted force constraint remains active. Assume that the resulting closed-loop quantities are differentiable with respect to κ . Using the signed-distance function in (1a), define the contact gap as

$$\Phi_{k+1}(\kappa) := \phi(z_{k+1}^*(\theta_k(\kappa), \kappa)), \quad (24)$$

where $z_{k+1}^*(\theta_k(\kappa), \kappa)$ is the next-step state component induced by the smoothed implicit contact dynamics. Suppose

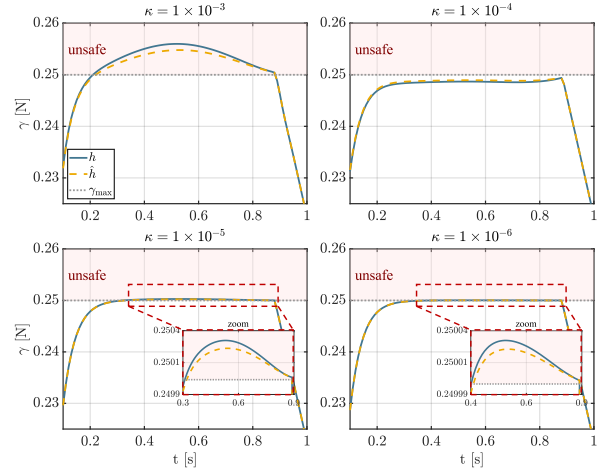


Fig. 5: Close-up view of the true and predicted contact force near the safety boundary under the CBF-QP for different values of the central-path parameter κ . The dotted grey line denotes the contact force limit γ_{\max} and the shaded region indicates the unsafe region ($\gamma > \gamma_{\max}$).

that the contact force and the closed-loop gap satisfy the local smoothed central path relation

$$\gamma_{k+1}(\kappa) > 0, \Phi_{k+1}(\kappa) > 0, \quad (25)$$

$$\gamma_{k+1}(\kappa)\Phi_{k+1}(\kappa) = \kappa. \quad (26)$$

Define the true next-step safety margin as

$$h_{k+1}(\kappa) := \gamma_{\max} - \gamma_{k+1}(\kappa), \quad (27)$$

and define the logarithmic closed-loop gap sensitivity as

$$A_\phi(\kappa) := \frac{d \log \Phi_{k+1}(\kappa)}{d \log \kappa} = \frac{\kappa}{\Phi_{k+1}(\kappa)} \frac{d \Phi_{k+1}(\kappa)}{d \kappa}. \quad (28)$$

Log-differentiating the central-path relation gives

$$\frac{dh_{k+1}}{d \log \kappa} = \gamma_{k+1}(\kappa) (A_\phi(\kappa) - 1), \quad (29)$$

or equivalently,

$$\frac{dh_{k+1}}{d \kappa} = \frac{\gamma_{k+1}(\kappa)}{\kappa} (A_\phi(\kappa) - 1). \quad (30)$$

Consequently, $A_\phi(\kappa) < 1$ implies that decreasing κ locally increases the true safety margin, whereas $A_\phi(\kappa) > 1$ implies that decreasing κ locally decreases the true safety margin. A first-order stationary point can occur when $A_\phi(\kappa) = 1$.

This local identity shows that reducing κ does not necessarily increase the true safety margin. A smaller κ would improve the margin only if the closed-loop gap remained fixed. In closed loop, however, this gap also changes with κ through the state, state increment, safety-filtered input, and smoothed contact update. This effect is captured by $A_\phi(\kappa)$. Therefore, the margin sensitivity has no fixed sign and depends on the sign of $A_\phi(\kappa) - 1$.

The results in Fig. 6 are consistent with this interpretation. Since $h_{k+1} = \hat{h}_{k+1} + \Delta h_k$, true safety requires the predicted margin to compensate for any negative approximation error. In Fig. 6(b), Δh approaches zero from below as κ decreases, but Fig. 6(c) shows that the predicted margin can also become small near the safety boundary. Thus, smaller κ alone is

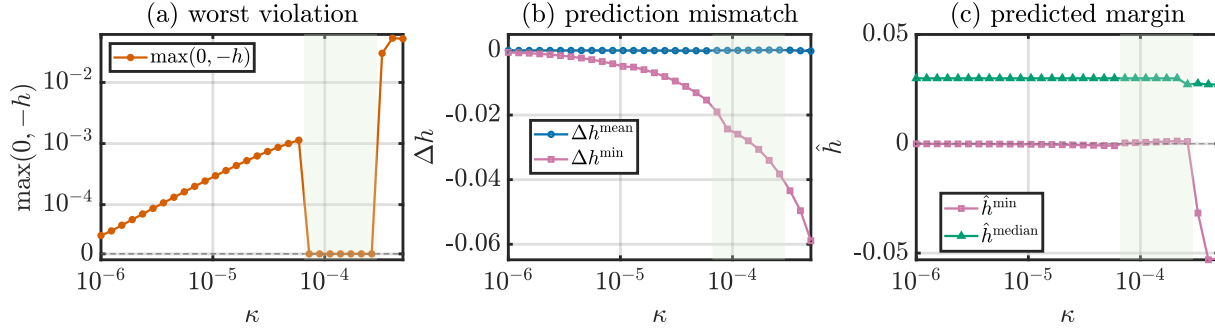


Fig. 6: Safety-related metrics across the central-path parameter κ . (a) Worst-case violation magnitude, $\max(0, -h)$. (b) Approximation error, $\Delta h := h - \hat{h}$, showing its mean and minimum values. (c) Predicted safety margin with minimum and median values. The shaded region indicates the non-violation interval of κ observed in simulation.

insufficient. For the tested system and candidate trajectory, the observed force safety behavior is most favorable at an intermediate κ , where approximation accuracy and margin preservation are balanced.

C. Boundary-Focused Screening of κ

The previous section shows that the true safety margin can vary non-monotonically with κ . Thus, κ should not be regarded merely as a numerical smoothing parameter, since it also influences the relaxed contact response and the resulting closed-loop safety behavior. This motivates a boundary-focused compatibility screening procedure for κ , summarized in Algorithm 1. The screening criterion compares the predicted margin with the observed one-step under-prediction near the safety boundary.

Algorithm 1 Boundary-Focused Screening of κ

Require: Candidates \mathcal{K} , rollouts \mathcal{P} , H, p, β

Ensure: κ^*

- 1: **for** $\kappa \in \mathcal{K}$ **do**
 - 2: Run CBF rollouts on \mathcal{P} and collect \hat{h}_{k+1}, h_{k+1}
 - 3: $\Delta h_k \leftarrow h_{k+1} - \hat{h}_{k+1}$
 - 4: $\rho_\kappa \leftarrow Q_{1-\beta}((-\Delta h_k)^+)$
 - 5: $S_p(\kappa) \leftarrow Q_p(\hat{h}_{k+1}) - \rho_\kappa$
 - 6: Compute $r_{\text{fail}}(\kappa)$
 - 7: **end for**
 - 8: $\mathcal{K}_{\text{comp}} \leftarrow \{\kappa \in \mathcal{K} : r_{\text{fail}}(\kappa) = 0, S_p(\kappa) \geq 0\}$
 - 9: **if** $\mathcal{K}_{\text{comp}} \neq \emptyset$ **then**
 - 10: $\mathcal{K}_{\text{score}} \leftarrow \arg \max_{\kappa \in \mathcal{K}_{\text{comp}}} S_p(\kappa)$
 - 11: $\kappa^* \leftarrow \min \mathcal{K}_{\text{score}}$
 - 12: **else**
 - 13: $\mathcal{K}_{\text{fail}} \leftarrow \arg \min_{\kappa \in \mathcal{K}} r_{\text{fail}}(\kappa)$
 - 14: $\mathcal{K}_{\text{score}} \leftarrow \arg \max_{\kappa \in \mathcal{K}_{\text{fail}}} S_p(\kappa)$
 - 15: $\kappa^* \leftarrow \min \mathcal{K}_{\text{score}}$
 - 16: **end if**
 - 17: **return** κ^*
-

The rollout set \mathcal{P} contains representative scenarios in which the closed-loop trajectory approaches the safety boundary within a short horizon H . For each candidate κ , the predicted margin \hat{h}_{k+1} enforced by the standard CBF-QP

and the corresponding true margin h_{k+1} obtained from the implicit contact dynamics are collected. Since safety depends on $h_{k+1} = \hat{h}_{k+1} + \Delta h_k$, negative values of Δh_k indicate that the predicted margin is optimistic. We therefore define

$$\rho_\kappa = Q_{1-\beta}((-\Delta h_k(\kappa))^+), \quad (31)$$

$$S_p(\kappa) = Q_p(\hat{h}_{k+1}(\kappa)) - \rho_\kappa, \quad (32)$$

where $Q_p(\cdot)$ denotes the empirical p -quantile of the collected rollout samples, and $(a)^+ := \max(a, 0)$ denotes the positive-part operator. Here, ρ_κ is the selected upper-tail under-prediction level, and $S_p(\kappa)$ measures whether the lower-tail predicted margin is large enough to compensate for the observed one-step under-prediction. The parameters p and β determine the lower-tail margin quantile and the upper-tail under-prediction quantile, respectively. The failure rate $r_{\text{fail}}(\kappa)$ is the proportion of rollouts that encounter implicit-solver failure.

A candidate is called compatible if it has no rollout failures and its compatibility score is nonnegative. The compatible set is

$$\mathcal{K}_{\text{comp}} = \{\kappa \in \mathcal{K} : r_{\text{fail}}(\kappa) = 0, S_p(\kappa) \geq 0\}. \quad (33)$$

If this set is nonempty, we select the compatible candidate with the largest compatibility score, choosing the smallest κ among candidates with equal scores. Otherwise, a candidate is chosen by first minimizing the failure rate, then maximizing the compatibility score among the remaining candidates, and finally choosing the smallest value of κ .

D. Robust Barrier Tightening Under Approximation Error

The screening procedure identifies a κ whose predicted margin is compatible with the observed one-step under-prediction. However, it does not remove the residual approximation error introduced by the local Taylor approximation of the implicit contact force. Consequently, satisfying the nominal discrete-time CBF constraint based on the predicted safety margin does not guarantee that the true safety margin is nonnegative.

As illustrated in Fig. 8, under-prediction is the safety-critical case because the predicted force can remain below the limit while the true force exceeds it.

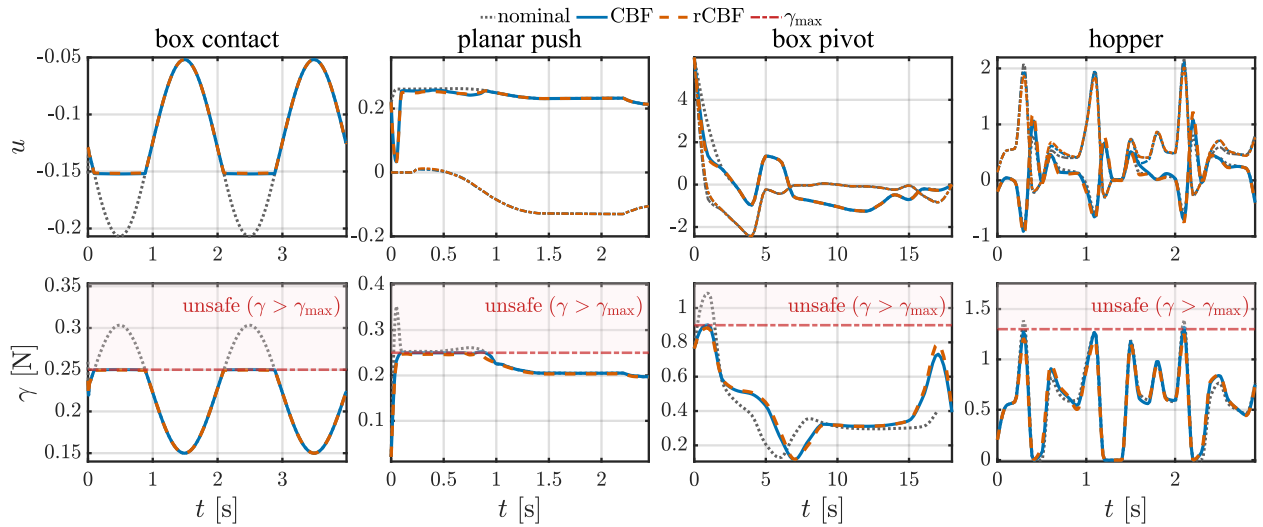


Fig. 7: Control and safety comparison across four systems. The top row shows the control inputs u for the box contact, planar push, box pivot, and hopper systems (from left to right), while the bottom row shows the corresponding safety metric γ . Black dotted curves denote the nominal controller, blue solid curves denote CBF, and orange dashed curves denote rCBF. The red dash-dotted line indicates γ_{\max} , and the shaded region marks unsafe operation ($\gamma > \gamma_{\max}$).

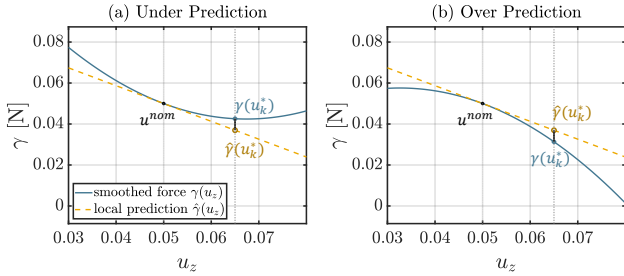


Fig. 8: One-step force prediction error. The local prediction $\hat{\gamma}$ around u^{nom} can under- or over-estimate the true force at u_k^* . Under-prediction is safety-critical because it may make an unsafe input appear feasible.

To account for this remaining one-step approximation error in (21), we bound Δh from below. Specifically, we consider a nonnegative κ -dependent tightening term δ_κ satisfying

$$-\delta_\kappa \leq \Delta h_k \quad (34)$$

over an operating region near the safety boundary.

Proposition 1 (Tightened CBF Constraint): Suppose that the approximation error satisfies (34) for some $\delta_\kappa \geq 0$. If the control input satisfies the tightened predicted CBF condition

$$\hat{h}_{k+1}(u_k; \kappa) \geq (1 - \alpha)h_k + \delta_\kappa, \quad (35)$$

then the true next-step safety margin satisfies

$$h_{k+1} \geq (1 - \alpha)h_k. \quad (36)$$

In particular, if $h_k \geq 0$ and $\alpha \in [0, 1]$, then $h_{k+1} \geq 0$.

Proof: Using (34), (35), and (22), we obtain

$$h_{k+1} = \hat{h}_{k+1} + \Delta h_k \geq (1 - \alpha)h_k + \delta_\kappa + \Delta h_k \geq (1 - \alpha)h_k. \quad (37)$$

If $h_k \geq 0$ and $\alpha \in [0, 1]$, then $(1 - \alpha)h_k \geq 0$, and hence $h_{k+1} \geq 0$. ■

Hence, when the approximation error bound in (34) holds, the tightened constraint guarantees that the true safety margin of the smoothed implicit model satisfies the nominal one-step barrier condition. In practice, an exact closed-form bound for δ_κ is generally unavailable. We therefore choose δ_κ conservatively from boundary-focused offline rollouts using statistics of the observed under-prediction $(-\Delta h_k)^+$, such as an upper quantile or the maximum.

As illustrated in Fig. 1, the same tightening idea can be conditionally extended to the unsmoothed model when the smoothing mismatch is also bounded. Let h_{k+1}^0 denote the safety margin of the unsmoothed model, corresponding to $\kappa = 0$. Then

$$h_{k+1}^0 = \hat{h}_{k+1} + \underbrace{(h_{k+1} - \hat{h}_{k+1})}_{\text{linearized error}} + \underbrace{(h_{k+1}^0 - h_{k+1})}_{\text{smoothed mismatch}}. \quad (38)$$

Thus, if

$$-\delta_{\text{lin}} \leq h_{k+1} - \hat{h}_{k+1}, \quad (39)$$

$$-\delta_{\text{smooth}} \leq h_{k+1}^0 - h_{k+1}, \quad (40)$$

then enforcing

$$\hat{h}_{k+1} \geq (1 - \alpha)h_k^0 + \delta_{\text{lin}} + \delta_{\text{smooth}} \quad (41)$$

implies

$$h_{k+1}^0 \geq (1 - \alpha)h_k^0. \quad (42)$$

Therefore, safety for the unsmoothed system requires bounding both the linearization error under the smoothed model and the smoothing mismatch between the smoothed and unsmoothed models.

The smoothing margin δ_{smooth} can be interpreted through the impulse-momentum relation. Recall that γ_{k+1} is the average contact force within time step k of duration T . Due to the conservation of momentum, the difference between the

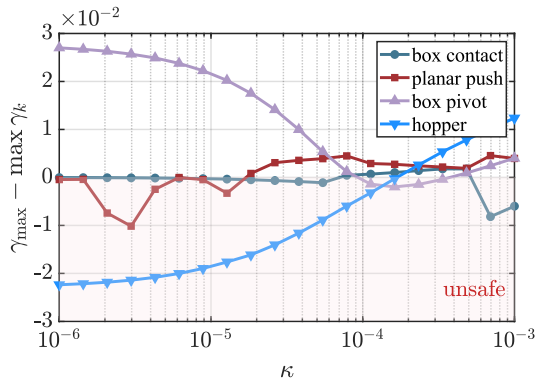


Fig. 9: κ -sweep results across four systems, showing the safety margin with unsafe regions shaded.

unsmoothed force γ_{k+1}^0 and the smoothed force γ_{k+1}^κ can be bounded as

$$\gamma_{k+1}^0 - \gamma_{k+1}^\kappa \leq \frac{m_{\text{eff}}}{T} |v_{n,k+1}^0 - v_{n,k+1}^\kappa|. \quad (43)$$

where m_{eff} is the effective mass along the contact normal, and $v_{n,k+1}^0$ and $v_{n,k+1}^\kappa$ denote the post-contact normal velocities under the unsmoothed and smoothed contact dynamics, respectively.

IV. EXPERIMENTS AND RESULTS

Four contact-rich robotic systems are used to evaluate the proposed CBF-based safety filtering method for implicit contact dynamics. The experiments are conducted on a 1D box contact, a planar push, a box pivot, and a hopper, as shown in Fig. 3. All systems impose the same form of force safety constraint, $\gamma_k \leq \gamma_{\max}$, and share the same implicit contact dynamics model and QP formulation. Reference trajectories are generated via trajectory optimization following [30]. A nominal PD controller is used to track these trajectories without explicit safety enforcement.

A. κ -Dependent Safety Behavior

To examine how κ affects safety violations, we evaluated each system for

$$\kappa_i \in \text{logspace}(10^{-6}, 10^{-3}, 20) \quad (44)$$

and recorded whether a safety violation occurred. Since safety violations also depend on the barrier gain α , we fix $\alpha = 0.95$ for all systems to enable a consistent comparison.

Fig. 9 shows that the relationship between κ and safety margin varies substantially across systems and is often non-monotonic. In the box contact system, an intermediate band of κ values leads to a safety violation, indicating that reducing κ does not necessarily improve safety. The box pivot results show a similar pattern, with safe behavior at both smaller and larger κ values but a safety violation near $\kappa \approx 10^{-4}$. The planar push also exhibits a non-monotonic trend, with substantial variation in safety margin across the tested range. In contrast, the hopper system shows a monotonic increase in safety margin as κ increases. These results suggest that non-violating κ values often form a range rather than a single optimal point, making κ screening nontrivial in practice.

TABLE I: Quantitative robust CBF comparison across four systems. Metrics are computed from deterministic rollouts for each controller. The force limits are $\gamma_{\max} = 0.25$ (box contact), 0.245 (planar push), 0.9 (box pivot), and 1.3 (hopper).

System	Controller	Viol.	Max over.	Peak.	Succ.
Box contact	Nominal	0.398	0.0533	0.3033	-
	CBF	0.345	0.0002	0.2502	-
	rCBF	0.000	0.0000	0.2497	-
Planar push	Nominal	0.340	0.0799	0.3249	-
	CBF	0.260	0.0000	0.2450	-
	rCBF	0.000	0.0000	0.2450	-
Box pivot	Nominal	0.056	0.1890	1.0890	Y
	CBF	0.053	0.0026	0.9026	N
	rCBF	0.000	0.0000	0.8851	Y
Hopper	Nominal	0.067	0.1017	1.4017	N
	CBF	0.033	0.0117	1.3117	N
	rCBF	0.000	0.0000	1.2225	Y

TABLE II: Sensitivity to fixed robust barrier tightening δ_κ on the hopper and planar push systems. The columns ρ_{85} and ρ_{90} denote the 85th and 90th percentiles of the one-step under-prediction samples $(-\Delta h_k)^+$ used to choose δ_κ , and max denotes the maximum observed under-prediction.

System	Metric	0	ρ_{85}	ρ_{90}	max
Hopper	Peak	1.3117	1.2713	1.2560	1.2186
	Viol.	0.033	0.000	0.000	0.000
	Dev.	0.0688	0.0827	0.0866	0.1015
	Succ.	N	Y	Y	Y
Planar push	Peak	0.2450	0.2450	0.2450	0.2450
	Viol.	0.260	0.020	0.000	0.000
	Dev.	0.0055	0.0055	0.0055	0.0055
	Succ.	N	N	Y	Y

B. Necessity of Robust CBF under Approximation Error

To evaluate the effect of approximation error on safety filtering, we compare the nominal controller, the standard CBF, and the proposed robust CBF on the same four contact-rich robotic systems using the κ value obtained from Algorithm 1. For each system, the barrier gain parameter α is fixed at 0.95. The selected κ^* and δ_{κ^*} are fixed before evaluation and are not tuned on the reported rollouts.

Fig. 7 compares the contact force trajectories produced by the standard CBF and the proposed robust CBF. Under the standard CBF, satisfying the linearized safety constraint in the CBF-QP does not always prevent force violations. Table I summarizes the quantitative comparison across all systems in terms of the violation rate (*Viol.*), the maximum force overshoot above the limit (*Max over.*), the peak contact force (*Peak.*), and task success (*Succ.*) for each controller. The standard CBF substantially reduces the magnitude of violations, but small residual violations can remain because of approximation error.

In these deterministic rollouts, the proposed robust CBF eliminates the observed contact force violations across all tested systems. It also improves task feasibility in the box-pivot and hopper examples, where the standard CBF fails to complete the task.

Table II shows the trade-off induced by the fixed robust margin δ_κ on the hopper and planar push systems. Here, *Dev.*

denotes the mean control deviation from the nominal input over the rollout, measured as $\|u - u^{\text{nom}}\|$. In both systems, increasing δ_κ improves safety but makes the control action more conservative. The required margin is system-dependent. On the hopper, ρ_{85} is sufficient to eliminate force violations, whereas on the planar push, residual violations remain at ρ_{85} and the tested rollout first becomes violation-free at ρ_{90} .

V. CONCLUSION

In this work, we presented a method for applying safety-critical control to systems governed by smoothed implicit contact dynamics by locally approximating the implicit contact force with a first-order Taylor expansion. Our analysis revealed that the central-path parameter κ , while improving numerical smoothness, has a nontrivial effect on safety. Although smaller κ reduces one-step approximation error, the resulting closed-loop safety behavior is non-monotonic because κ changes both the relaxed contact response and the safety-filtered closed-loop trajectory.

This insight motivated two practical design components. First, we use a boundary-focused κ -screening method to identify reliable smoothing parameters. Second, we use a robust CBF formulation with a tightening margin to reduce approximation-induced safety violations. These results show that contact smoothing should be treated not only as a numerical device but also as a safety-relevant design parameter in contact-rich control. We expect this perspective to support the more reliable use of implicit contact dynamics in safety-critical robotic applications.

REFERENCES

- [1] A. Patel, S. L. Shield, S. Kazi, A. M. Johnson, and L. T. Biegler, "Contact-implicit trajectory optimization using orthogonal collocation," *IEEE Robotics and Automation Letters*, vol. 4, no. 2, pp. 2242–2249, 2019.
- [2] F. R. Hogan and A. Rodriguez, "Feedback control of the pusher-slider system: A story of hybrid and underactuated contact dynamics," in *Algorithmic Foundations of Robotics XII: Proceedings of the Twelfth Workshop on the Algorithmic Foundations of Robotics*. Springer, 2020, pp. 800–815.
- [3] A. K. Valenzuela, "Mixed-integer convex optimization for planning aggressive motions of legged robots over rough terrain," Ph.D. dissertation, Massachusetts Institute of Technology, 2016.
- [4] F. R. Hogan and A. Rodriguez, "Reactive planar non-prehensile manipulation with hybrid model predictive control," *The International Journal of Robotics Research*, vol. 39, no. 7, pp. 755–773, 2020.
- [5] M. Posa, C. Cantu, and R. Tedrake, "A direct method for trajectory optimization of rigid bodies through contact," *The International Journal of Robotics Research*, vol. 33, no. 1, pp. 69–81, 2014.
- [6] G. Kim, D. Kang, J.-H. Kim, S. Hong, and H.-W. Park, "Contact-implicit model predictive control: Controlling diverse quadruped motions without pre-planned contact modes or trajectories," *The International Journal of Robotics Research*, vol. 44, no. 3, pp. 486–510, 2025.
- [7] Y. Shirai, D. K. Jha, and A. U. Raghunathan, "Robust pivoting manipulation using contact implicit bilevel optimization," *IEEE Transactions on Robotics*, vol. 40, pp. 3425–3444, 2024.
- [8] H. Lee, Y. Kim, V. M. Staven, and C. Sloth, "Trajectory optimization for in-hand manipulation with tactile force control," in *2025 IEEE/RSJ International Conference on Intelligent Robots and Systems (IROS)*, 2025, pp. 21 773–21 779.
- [9] H. J. T. Suh, T. Pang, and R. Tedrake, "Bundled gradients through contact via randomized smoothing," *IEEE Robotics and Automation Letters*, vol. 7, no. 2, pp. 4000–4007, 2022.
- [10] T. A. Howell, S. Le Cleac'h, J. Z. Kolter, M. Schwager, and Z. Manchester, "Dojo: A differentiable simulator for robotics," *arXiv preprint arXiv:2203.00806*, vol. 9, no. 2, p. 4, 2022.
- [11] T. Pang, H. T. Suh, L. Yang, and R. Tedrake, "Global planning for contact-rich manipulation via local smoothing of quasi-dynamic contact models," *IEEE Transactions on Robotics*, vol. 39, no. 6, pp. 4691–4711, 2023.
- [12] H. T. Suh, T. Pang, T. Zhao, and R. Tedrake, "Dexterous contact-rich manipulation via the contact trust region," *The International Journal of Robotics Research*, p. 02783649251398875, 2025.
- [13] V. Kurtz, A. Castro, A. Ö. Önel, and H. Lin, "Inverse dynamics trajectory optimization for contact-implicit model predictive control," *The International Journal of Robotics Research*, vol. 45, no. 1, pp. 23–40, 2026.
- [14] X. Wang, J. Yang, J. Mao, S. Li, and Y. Yan, "Guarding force: Safety-critical compliant control for robot-environment interaction," *IEEE Robotics and Automation Letters*, vol. 11, no. 1, pp. 930–937, 2025.
- [15] F. Vinter-Hviid, C. Sloth, T. R. Savarimuthu, and I. Iturrate, "Safe contact-based robot active search using bayesian optimization and control barrier functions," *Frontiers in Robotics and AI*, vol. 11, p. 1344367, 2024.
- [16] Y. Kim, J. Kim, A. H. Li, A. D. Ames, and C. Sloth, "Robust adaptive safe robotic grasping with tactile sensing," in *2025 European Control Conference (ECC)*, 2025, pp. 2531–2538.
- [17] X. Xu, P. Tabuada, J. W. Grizzle, and A. D. Ames, "Robustness of control barrier functions for safety critical control," *IFAC-PapersOnLine*, vol. 48, no. 27, pp. 54–61, 2015.
- [18] M. Jankovic, "Robust control barrier functions for constrained stabilization of nonlinear systems," *Automatica*, vol. 96, pp. 359–367, 2018.
- [19] Y. Hu, L. Anderson, T.-M. Li, Q. Sun, N. Carr, J. Ragan-Kelley, and F. Durand, "DiffTaichi: Differentiable programming for physical simulation," *arXiv preprint arXiv:1910.00935*, 2019.
- [20] M. Geilinger, D. Hahn, J. Zehnder, M. Bäcker, B. Thomaszewski, and S. Coros, "Add: Analytically differentiable dynamics for multi-body systems with frictional contact," *ACM Transactions on Graphics (TOG)*, vol. 39, no. 6, pp. 1–15, 2020.
- [21] M. Lee, J. Lee, and D. Lee, "Differentiable dynamics simulation using invariant contact mapping and damped contact force," in *2023 IEEE International Conference on Robotics and Automation (ICRA)*, 2023, pp. 11 683–11 689.
- [22] S. Le Cleac'h, T. A. Howell, S. Yang, C.-Y. Lee, J. Zhang, A. Bishop, M. Schwager, and Z. Manchester, "Fast contact-implicit model predictive control," *IEEE Transactions on Robotics*, vol. 40, pp. 1617–1629, 2024.
- [23] A. D. Ames, S. Coogan, M. Egerstedt, G. Notomista, K. Sreenath, and P. Tabuada, "Control barrier functions: Theory and applications," in *2019 18th European Control Conference (ECC)*, 2019, pp. 3420–3431.
- [24] A. Agrawal and K. Sreenath, "Discrete control barrier functions for safety-critical control of discrete systems with application to bipedal robot navigation," in *Robotics: Science and Systems*, vol. 13. Cambridge, MA, USA, 2017, pp. 1–10.
- [25] J. Zeng, B. Zhang, and K. Sreenath, "Safety-critical model predictive control with discrete-time control barrier function," in *2021 American Control Conference (ACC)*, 2021, pp. 3882–3889.
- [26] T. D. Son and Q. Nguyen, "Safety-critical control for non-affine nonlinear systems with application on autonomous vehicle," in *2019 IEEE 58th Conference on Decision and Control (CDC)*, 2019, pp. 7623–7628.
- [27] J. Seo, J. Lee, E. Baek, R. Horowitz, and J. Choi, "Safety-critical control with nonaffine control inputs via a relaxed control barrier function for an autonomous vehicle," *IEEE Robotics and Automation Letters*, vol. 7, no. 2, pp. 1944–1951, 2022.
- [28] W. Xiao, R. Allen, and D. Rus, "Safe neural control for non-affine control systems with differentiable control barrier functions," in *2023 62nd IEEE Conference on Decision and Control (CDC)*, 2023, pp. 3366–3371.
- [29] U. Dini, *Lezioni di analisi infinitesimale...: Calcolo differenziale. 1907. di. 720 p.* Fratelli Nistri, 1907, vol. 1.
- [30] T. A. Howell, S. Le Cleac'h, S. Singh, P. Florence, Z. Manchester, and V. Sindhvani, "Trajectory optimization with optimization-based dynamics," *IEEE Robotics and Automation Letters*, vol. 7, no. 3, pp. 6750–6757, 2022.